Manuscript version: 29 May 2020
Elsevier, Materials Today Communications
https://doi.org/10.1016/j.mtcomm.2020.101294

Comprehensive assessment of spatter material generated during selective laser melting of stainless steel

Muhannad Ahmed Obeidi [a, b, c, *, 1], ***Andre Mussatto*** [a, b, c, *] ***Robert Groarke*** [a, b, c], ***Rajani K. Vijayaraghavan*** [a, c, d], ***Alex Conway*** [f], ***Frederico Rossi Kaschel*** [g], ***Eanna McCarthy*** [b, c], ***Owen Clarkin*** [b], ***Robert O'Connor*** [a, c, e], ***Dermot Brabazon*** [a, b, c]

[a] I-Form Advanced Manufacturing Research Centre, Dublin City University, Dublin 9, Ireland
[b] School of Mechanical & Manufacturing Engineering, Dublin City University, Dublin 9, Ireland
[c] Advanced Processing Technology Research Centre, Dublin City University, Dublin 9, Ireland
[d] School of Electronic Engineering, Dublin City University, Dublin 9, Ireland
[e] School of Physical Sciences, Dublin City University, Dublin 9, Ireland
[f] AMBER Research Centre, Science and Technology in Advanced Manufacturing Research Group (STAM), Trinity College Dublin, Ireland
[g] I-Form Advanced Manufacturing Research Centre, University College Dublin, Dublin 4, Ireland
[*] The authors have made an equal contribution to the article.
[1] Corresponding Author: muhannad.ahmedobeidi@dcu.ie

Abstract

Laser-powder interaction and meltpool dynamics govern the physics behind the selective laser melting process. Spattering is an unavoidable phenomenon taking place during the process which is known to influence the integrity of the interaction between the incident laser beam and change the powder bed characteristics. This can consequently have a negative effect on final part integrity and quality of recycled powder. Hence, it is crucial to assess the characteristics of spatter particles to avoid the printing of defective parts. This work reports a detailed characterisation of spatter matter generated during selective laser melting of stainless steel. To better assess the characteristics of the spatter, the spattered material was benchmarked against the virgin powder. The results show no microstructural differences. However, the spatter morphological, chemical, optical and physical properties assessed in this work differ from the virgin powder. The results presented in this work are of significant contribution to the powder bed fusion field of additive manufacturing as it provides a unique insight to the characteristics of spatter matter generated from the processing of 316L stainless steel powder.

Keywords: Metal additive manufacturing; Spatter; Powder oxidation; Powder recycling; Stainless steel powder; Selective laser melting; Powder bed fusion

To cite this article: *Muhannad Ahmed Obeidi, Andre Mussatto, Robert Groarke, Rajani K. Vijayaraghavan, Alex Conway, Frederico Rossi Kaschel, Eanna McCarthy, Owen Clarkin, Robert O'Connor, Dermot Brabazon, Comprehensive assessment of spatter material generated during selective laser melting of stainless steel, Materials Today Communications 25 (2020) 101294.*

1. Introduction

In additive manufacturing, several types of metal powders are used in the manufacturing of engineered parts. It uses a layering approach to building up materials layer by layer based on a computer aided designed model [1–3]. In the recent years, this process has grown rapidly and has been recognised and adopted by numerous industries including aerospace, automotive, biomedical, oil and gas and machine tool manufacturing industries [4–6]. Moreover, additive manufactured parts are not only represented by prototype parts anymore but customised and functioning end-use parts which can support extremely high mechanical loads. These parts can be manufactured in extremely complex geometries which would be difficult or impossible to be produced by using the traditional manufacturing methods such as casting and machining [7,8]. This process is growing exponentially with a very promising future of more applications yet to be discovered [9–16]. The additive manufactured parts can be produced from pure metals or from metal matrix composites such as metal alloys and ceramics reinforced metal powders [17–22].

Several studies have been done on the processing of different metals and alloy powders like steel, Inconel, titanium, AlSi12Mg and Si10Mg via metal additive manufacturing [23–26]. The powder bed fusion metal additive manufacturing technique, also known as selective laser melting is one of the most commonly used processes in metal additive manufacturing. As a thermal process, a heat source, laser or electron beam is used to melt the metal powder in selective locations indicated by the Computer-aided design file. When the laser beam fuses a particular powder layer, it also partially melts the previous layer in order to create full bonding of the consecutive layers until the entire part is completed. Some of the unfused, partially melted and fully melted powder particles surrounding the part can be ejected above the meltpool and the powder bed. The molten material is then solidified forming a very specific morphology due to its dynamics and the chamber conditions. The formation and ejection of this melted/partially melted material has a significant degradative effect on the quality of the additively manufactured parts. The spattering phenomenon is unavoidable and the deposition of the spattered matter in the consecutive layers can lead to the presence of pores, voids and other defects in printed parts [27]. This can be explained by the larger, partially welded and satellite powder particles formed during the molten metal ejection. The spatter affected

particles may require higher or lower laser power levels than that defined in the chosen process parameters. Typically, this is because the morphology, surface chemistry and the laser absorption properties of the spattered powder may differ from the virgin powder. Excessive and incomplete melting or even lack of fusion may result from printing with such a powder [28,29].

Several researchers have investigated spatter generation phenomenon and reported that the effect of the metal vapour expansion is the main reason for the ejection and spattering of the powder particles [30–32]. Other studies [33–36] used mathematical models, such as finite element analysis, simulations and high-speed cameras to validate experimental results. These investigations reported that the ejected powder particles are highly affected by the laser power applied, the scanning speed and the amount of metal vapour and plasma formed above the meltpool. It was also reported that spatter and condensate do in fact deposit on the powder bed layer being lased [37]. The inert gas flow velocity does impact on spatter trajectory and it was reported that higher gas velocities increase the transport of spatter resulting in a more even distribution downstream of the gas flow rather than along the scanning direction [38]. Yang et al. studied the spatter behaviour and its influences on printed parts, their findings indicate that spatter significantly reduces the mechanical properties of parts [39]. Another study found that part surface roughness increases in the spatter rich region of the building area, hence preventing of the manufacture of high quality parts [40]. Despite the fact that there is a reasonable number of research in this area, significant gaps in current knowledge particular relating to spatter analysis for 316L stainless steel, a widely used feedstock material still exist. Therefore, more in depth research needs to be performed to thoroughly understand the characteristics of laser spatter and its potential impact on the selective laser melting process.

The formation of spatter in selective laser melting generates a new powder system. Understanding how it differs from the virgin powder can assist on avoiding detrimental effect on parts. Therefore, the present study comprises a comprehensive assessment of spatter material generated during selective laser melting of 316L stainless steel.

2. Materials and Experimental Method

2.1 Powders

Commercially available gas atomised 316L stainless steel powder from Carpenter Additive was used in this study. The powder was supplied having a mean particle size of 30 µm and the chemical composition shown in Table 1.

Table 1 lists the chemical properties of the gas atomized 316L stainless steel (wt%).

C	Cr	Cu	Mn	Mo	Ni	N	O	P	Si	S	Fe
0.03	17.6	0.02	0.66	2.38	12.5	0.09	0.03	0.007	0.65	0.006	Bal.

2.2 Powder Sampling Strategy

Figure 1 shows the AconityMini system with the main locations where the powder samples were collected. The internal dimensions of the build chamber are 300×650×80 mm, the build volume dimension is 140 mm diameter × 200 mm height. The machine is an open access powder bed fusion system manufactured by Aconity3D Aachen, Germany. It is equipped with a 200 W fibre laser system of 1068 nm wavelength; model YLR-200-AC from IPG Laser GmbH, Carl-Benz-Strasse, Germany.

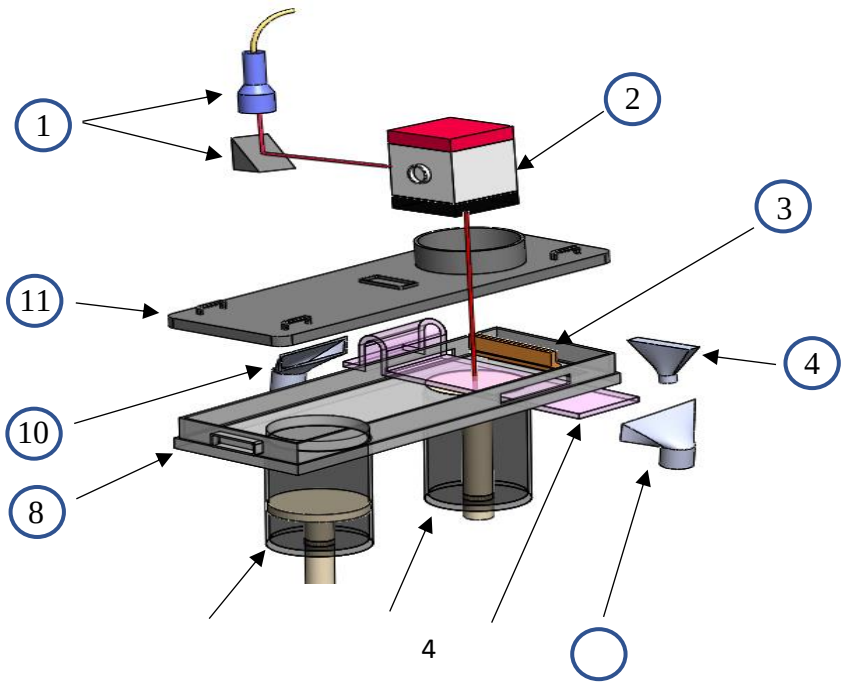

Figure 1 Schematic diagram of the Aconity Mini build chamber showing the main features of the 3D metal printer and the locations where the metal powder was collected. (1) laser beam collimator and optics, (2) 3D scanner, (3) powder deposition and re-coater slider, (4) overflow powder collector, (5) argon gas stream, (6) build platform, (7) powder supply, (8) build chamber enclosure, (9) argon gas inlet elbow, (10) argon gas outlet and (11) build chamber cover.

The metal printer is equipped with an oxygen sensor and continuous monitoring with a resolution of less than 20 ppm. The process is started by loading the powder into the powder supply (7), closing the build chamber cover (10) and purging the build chamber with argon gas purity of 99.999%. The argon gas is circulated through the printer system by means of a circulation fan. The gas enters the build chamber at the right-hand side of the build plate via elbow and window (4), passes over the top of the build platform and exits through window and elbow at the left of the build chamber (9). The exhaust gas is then forced through the cyclone filtration unit. In this unit, the contaminated powder particles which were exposed to the laser beam and suspended in the gas stream are filtered and the filtered gas is pumped back to the build chamber in addition to a controlled virgin gas flow.

The metal powders under study were collected from the as-supplied powder container (virgin powder), around the printed part and near the argon gas outlet (spattered powder) and from the powder overflow container (recycling powder).

2.3 Laser Processing Energy

AM is a thermal process and in order to produce a better understanding of the thermal energy applied to the material, it is essential to identify the relevant processing parameters. The main processing parameters which have the most significant effect on the fused and adjacent powder particles are the laser beam power (W), the scanning speed (mm/s), the laser beam spot size (mm), the hatch spacing (mm) and the applied powder layer thickness (mm). Moreover, it is very important to adopt unified technical terms in which this thermal energy is precisely described so that its effect on the produced part and the recycled powder can be characterised and differentiated between different metal printers. In this study, the thermal energy applied can be described and calculated in the following three terms and their values:

- The linear thermal energy $= \frac{\text{laser beam power (W)}}{\text{Scanning speed } (\frac{\text{mm}}{\text{s}})} = 0.2$ J/mm. which describes the thermal energy applied in a straight line of melting.
- The surface energy density $= \frac{\text{laser beam power (W)}}{\text{Scanning speed } \left(\frac{\text{mm}}{\text{s}}\right) \times \text{Hatch spacing (mm)}}$ 2.67 J/mm^2.
- The volumetric energy density = $\frac{\text{laser beam power (W)}}{\text{Scanning speed } \left(\frac{\text{mm}}{\text{s}}\right) \times \text{ Hatch spacing (mm)} \times \text{Layer thickness (mm)}} = 89$ J/mm^3

The total printing time was approximately ten hours with a surface area ratio of (layer area/total build area) 0.2 in a layer thickness of 30 microns and a total number of layers of 250.

2.4 Powder Characterisation

The physical characteristics of the powders used were analysed using a scanning electron microscope (SEM) Zeiss EVO LS-15, Malvern Mastersizer 3000 particle size analyser, Micromeritics AccuPyc 1330 Pycnometer and a Micromeritics Gemini VII 2390 BET (Brunauer–Emmett–Teller) surface area analyser. Micro-CT scanning was used to investigate the internal porosity of the metal powders. Computed tomography measurements were obtained using a Phoenix Nanotom system. Scanning took approximately 18 minutes at 165 kV. Under these scanning conditions the system has a resolution of 5.11 µm. The processing of the CT image data was carried out using VG studio Max 3.2. Phoenix DatosX. The powder bulk and surface chemical composition was investigated using energy dispersive X-ray (EDX) analysis coupled into a Hitachi S5500 Field Emission SEM and the X-ray photoelectron spectroscopy (XPS) was carried out using a conventional Mg Kα (hυ = 1486.6 eV) X-ray source in conjunction with a VG Microtech electron energy analyzer operating at a pass energy of 20 eV and at a pressure of $1x10^{-9}$ mbar, yielding an overall resolution of 1.2Ev. Prior to the analysis the samples were heated to 300 °C under nitrogen atmosphere to remove any moisture. Peak fitting analysis was carried out using the CasaXPS version 2.3.22 software. Light spectrometry was conducted to measure the reflection of the white light from the powders using an in-house developed system equipped with an Ocean Optics LS-1-CAL-INT Series Calibration Light Source and a Maya2000 Pro spectrometer. The crystal structure and phase analysis of the powder samples were carried out using a triple-axis Jordan Valley Bede D1 high resolution X-ray diffraction (XRD) system using a Cu-Kα (λ=1.5405 Å) radiation source operated at 45 kV and 40 mA.

3. Results and Discussion

3.1 Physical Characterisation of Powders

Figure 2 (a) shows an optical image comparing the colour of the powders. Significant differences in colour between the virgin and spattered powders is evident. The golden coloration of the spattered powder is caused by the interaction of the virgin powder with the laser and the chamber atmosphere. The morphology of the virgin powder is illustrated in Figure 2 (b). It shows a typical gas atomised morphology with good sphericity, as well as some elongated and satellite containing particles. The spattered powder and the powder affected by

spatter particles are distinguished in Figure 2 (c). Morphologically different from the virgin powder, the spatter is characterised by spatter and virgin powder fusion leading to significant numbers of satellite particles and large powder aggregations. A powder with such characteristics may fall onto the powder bed during the printing and prevent the next layer of powder from being deposited uniformly and may also cause internal defects in printing parts, as noted earlier. Another concern is that spattered powder will affect the recyclability and re-usage of powder.

(a)

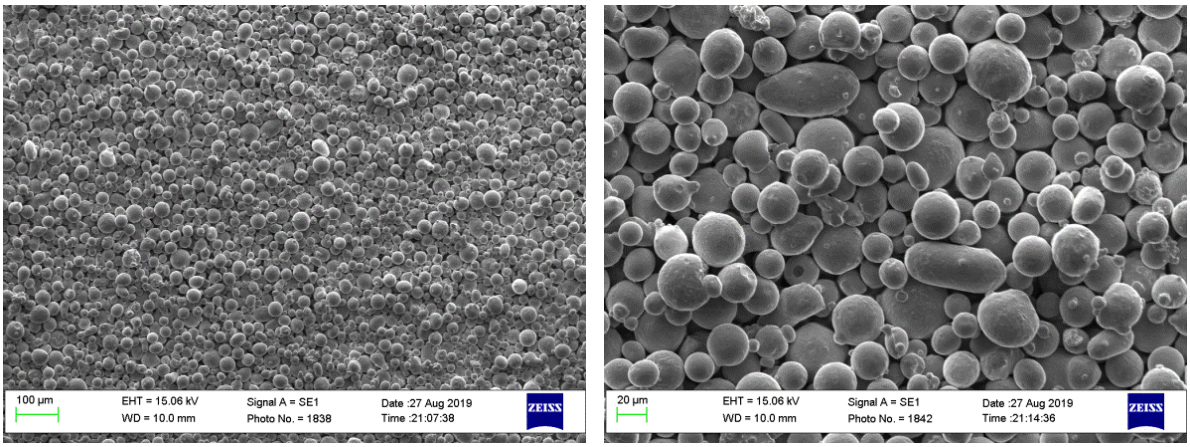

(b)

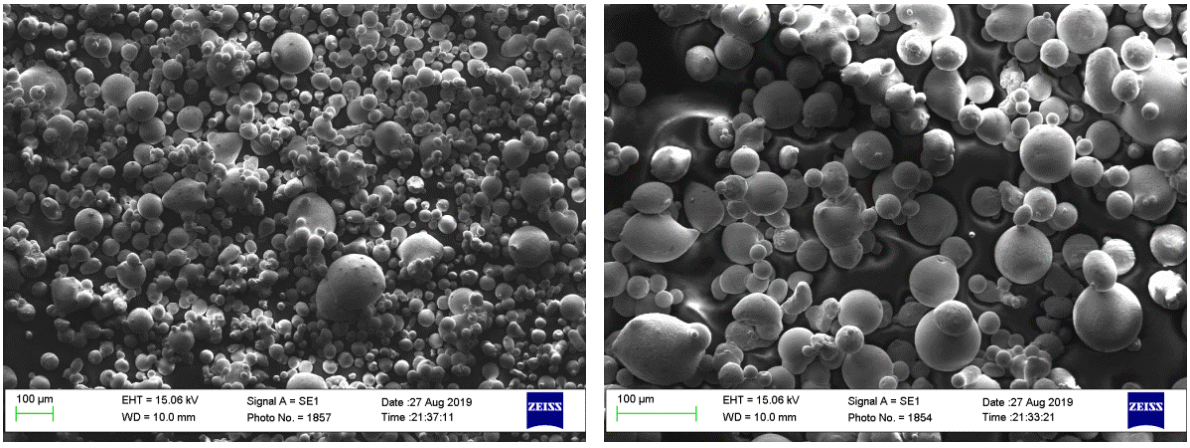

(c)

Figure 2 (a) Optical image compares the coloration of the virgin and spattered powder, (b) SEM image shows the morphology of the virgin powder and (c) of the spattered powder.

The original particle size distribution of the virgin powder is visibly altered by the presence of the spatter particles. Figure 3 shows the effect of satellite particles and aggregations caused by spatter on the virgin powder particle size distribution. A noticeable reduction of the volume of particles representing the mean virgin powder particle size is observed along with the

emergence of a wider particle size distribution due to satellite particles and aggregations. It is very important to note that the formation of smaller particles is not evident. This would tend to suggest that molten spatter particles are most likely to fuse during flight with other powder particles or fuse with the powder in the powder bed than breaking up to form smaller particles.

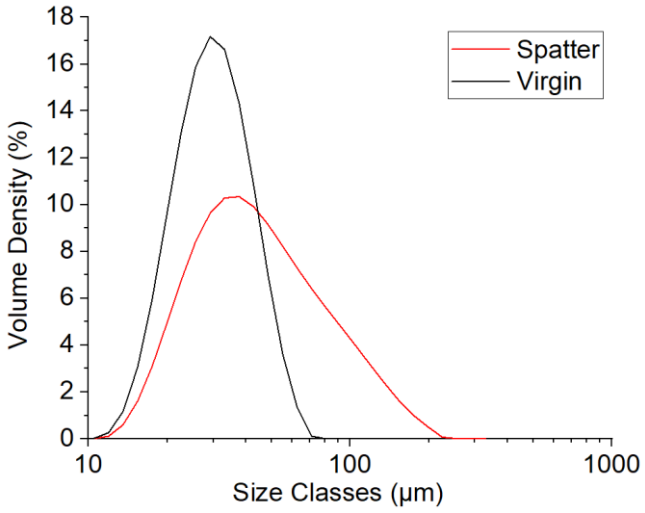

Figure 3 Plot comparing the particle size distribution of the virgin and spatter stainless steel powders.

Powder particles collected from the recycling unit of the printer, location illustrated in Figure 1 as (4) overflow powder collector, are shown in Figure 4. Figure 4 (a) shows micrographs of the powder collected from the recycling unit which was sieved to < 50μm, (b) shows only those particles > 75μm and (c) particles > 90μm. These micrographs clearly show the morphological change undergone by the virgin powder due to spattering, and it supports the previous discussion on particle size distribution. Figure 4 (a) shows evidence of satellite particles. However, as seen in Figure 2 (b) some satelliting is expected from the atomisation process. As seen in Figure 4 (b), that at this size range, particle aggregation is prevalent, whereas for the size classification of Figure 4 (c) micro and nano spattered satellites as well as particle-to-particle fusion are more prevalent. In general, any morphological change of the virgin powder found in the powder recycling unit should be addressed appropriately as the use of recycled powders containing spatter affected particles can lead to printing defects in parts [41].

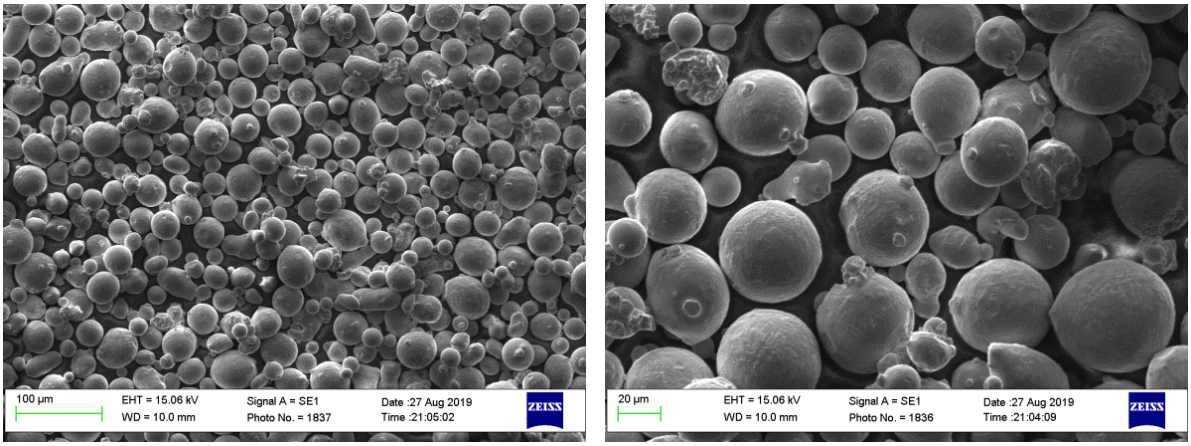

(a)

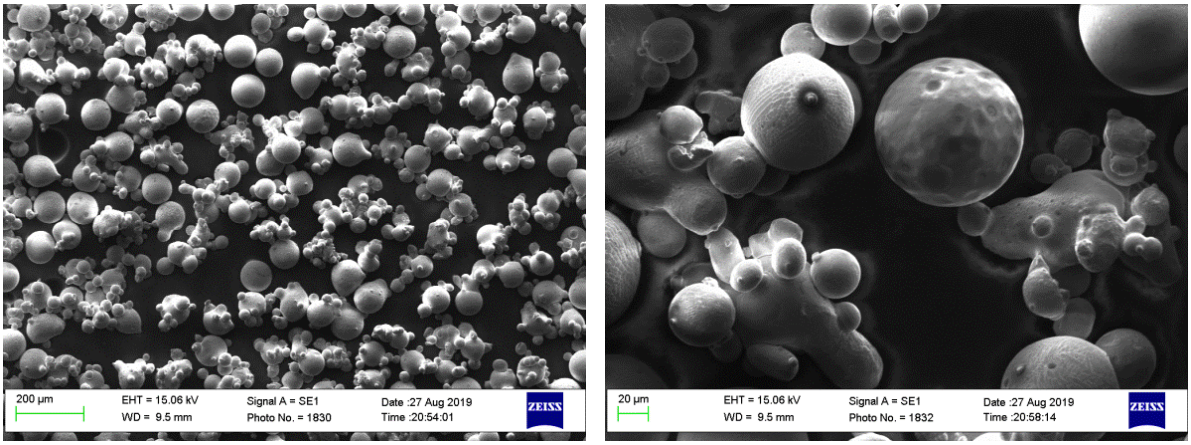

(b)

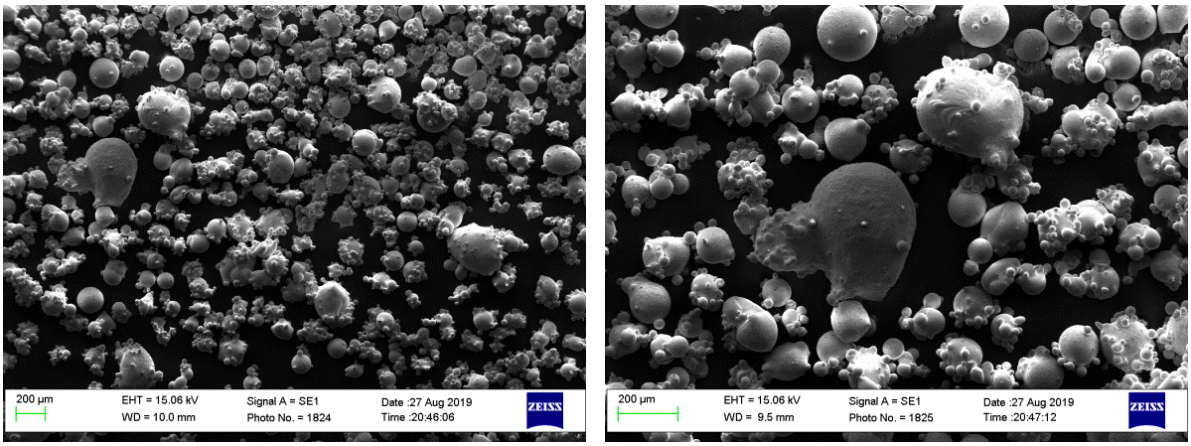

(c)

Figure 4 Shows micrographs of the powder collected from the recycling unit sieved to < 50 µm (a), recycling unit powder sieved to > 75 µm (b) and recycling unit powder sieved to > 90 µm (c).

Powder with closed internal porosity containing entrapped gasses or other contaminants can be detrimental for part formation [42]. The reduction of nearly 1% in density seen from the comparison between the virgin and spattered powder could be due to this effect. Porosity measurements are presented in Table 2. The results also show that the spattered powder presented slightly higher volume, which is to be expected. The BET evaluation revealed a

significant specific surface area difference between the powders. It seen that the specific surface area of the spattered powder is approximately twice of that of the virgin powder. This is because small particles have larger specific surface area than large particles. Hence, the reason for the larger specific surface area of the spattered powder is because that during the laser scanning of the powder bed, the virgin powder irradiated by the laser melt and due to various phenomena within the meltpool molten spatter fuse with other in-flight spatter or powder bed particles forming aggregates. It is also seen that heat affected particles can present grain type structure onto their surfaces and that spatters are rough and irregular shaped, hence both contribute to the increase of the specific surface area observed. The spattered material ejected from the meltpool is smaller than virgin powder particles, as seen above in Figure 4, leading to formation of small matter satellites onto the powder from the powder bed. This may also be considered a problem for the reasons that very small (nano scale) satellite matter may require less laser energy density to achieve melting than the ordinary particles size of the virgin powder.

Table 2 Illustrate the changes on the density, volume and surface area of the virgin stainless steel powder in comparison to the spattered powder of the same material.

Powder	Density (g/cm^3)	Volume (cm^3)	BET (m^2/g)
Virgin	$7.8385_{\pm 0.0241}$	$1.2758_{\pm 0.0039}$	$0.0242_{\pm 0.0020}$
Spatter	$7.7847_{\pm 0.0121}$	$1.2846_{\pm 0.0020}$	$0.0549_{\pm 0.0013}$

Figure 5 shows images of the X-ray computed tomography porosity analysis on the spattered particles. The existence of closed porosity is clear from Figure 5 (b-c). This explains the fact for the lower density of the spatter particles reported above. However, porosity is only seen inside very large aggregated spatters. A possible explanation for this is that during the flight and collision of molten spatters fumes and gases got trapped inside spatter aggregates. On the other hand, there is no evidence of porosity in those spatter particles less affected by aggregation. From Figure 5 (a) it seen the detrimental effect of spatter on the virgin powder morphology. Both the affected virgin powder and the aggregates contain numerous satellites and extremely rough textures. These are the two main reasons for the spatter particles large specific surface area.

https://doi.org/10.1016/j.mtcomm.2020.101294

(a)

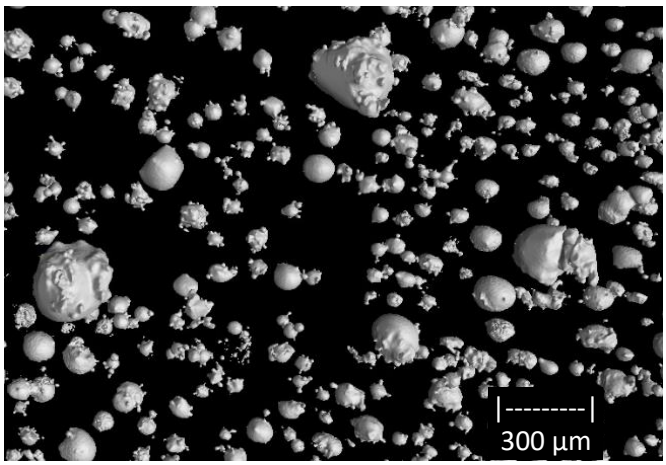

(b)

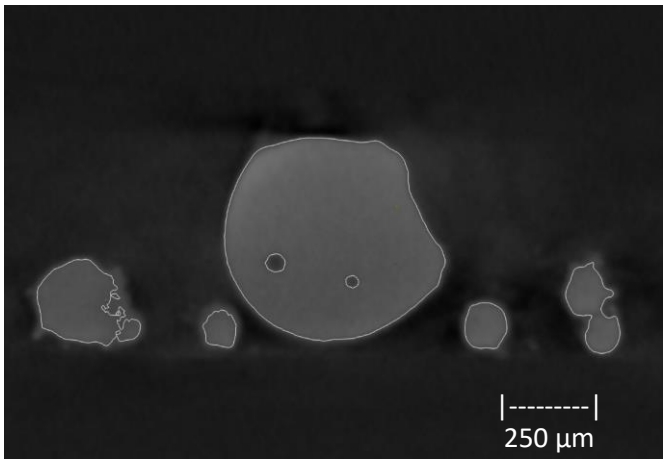

(c)

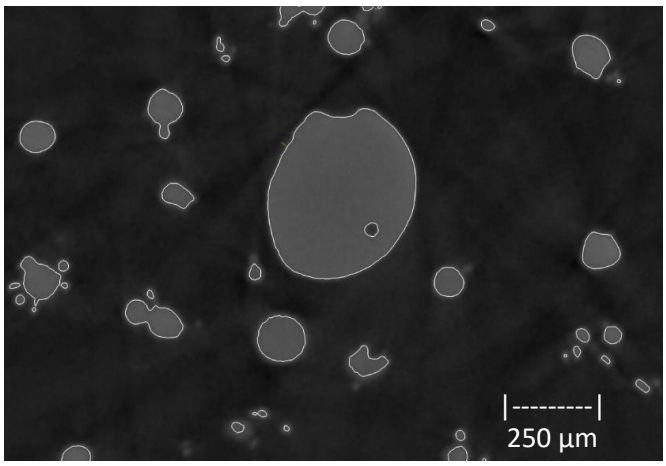

Figure 5 X-ray computed tomography porosity analysis of spattered particles: (a) spattered particles; (b-c) cross section images showing the existence of closed pores.

3.2 Chemical Analysis of Powders

The EDX analysis of the powder surface elemental compositions were performed with an accelerating voltage of 10kV and emission current of 10µA in an aperture diameter of 100µm. Monte Carlo (Casino v3.3) simulation of the possible path of secondary electron ionisation predicted a maximum penetration depth of 100nm. Figure 6 illustrates the results of the EDX

analysis of 316L virgin powder and spattered particles. Acknowledging the limitations of EDX detection performance for light elements, the results show significant evidence of altered surface chemical composition between the virgin 316L powder and spattered particles. The atomic percentage of Fe, Ni and Cr, the main elements in 316L, changed substantially in the spattered powder. Furthermore, a large increase in the oxygen content was measured. It is evident that oxygen increased in the spattered particles in comparison to the virgin 316L powder. This is potentially due to the molten metal from the melting pool spattering upwards and coming into contact and reacting with the remaining oxygen and fumes in the building chamber which allow the generation of oxides.

(a)

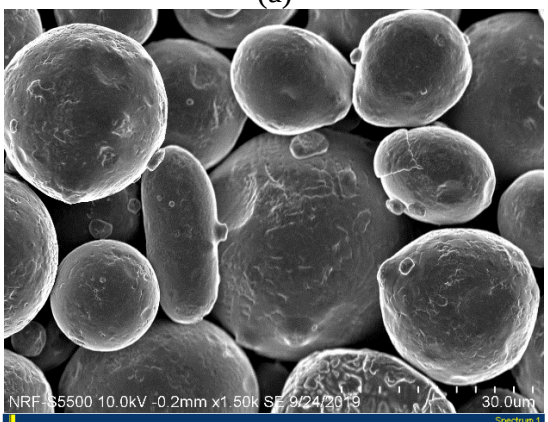

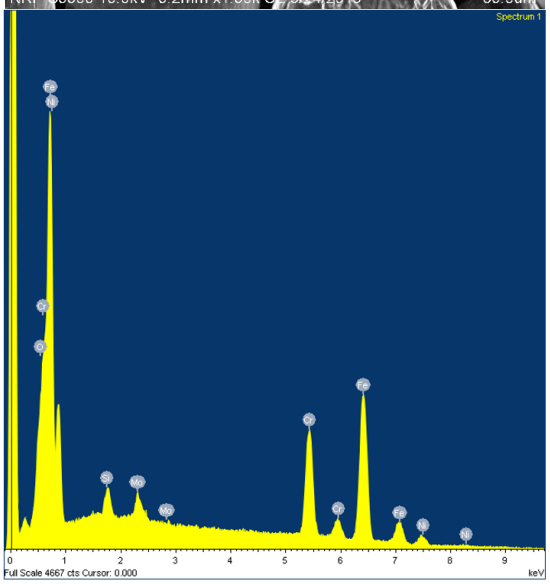

Element	Atomic%
Fe	55.37
Ni	17.55
Cr	13.15
O	4.20
Si	1.51
Mo	1.12

(b)

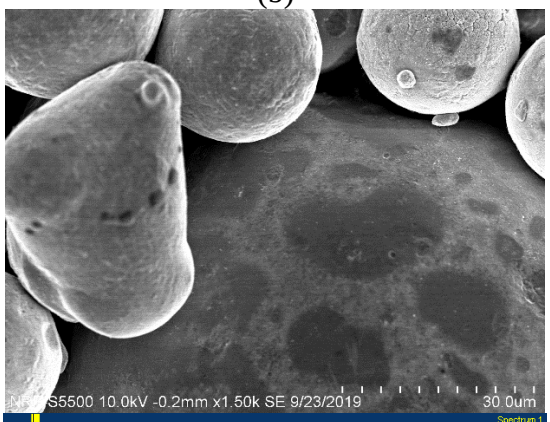

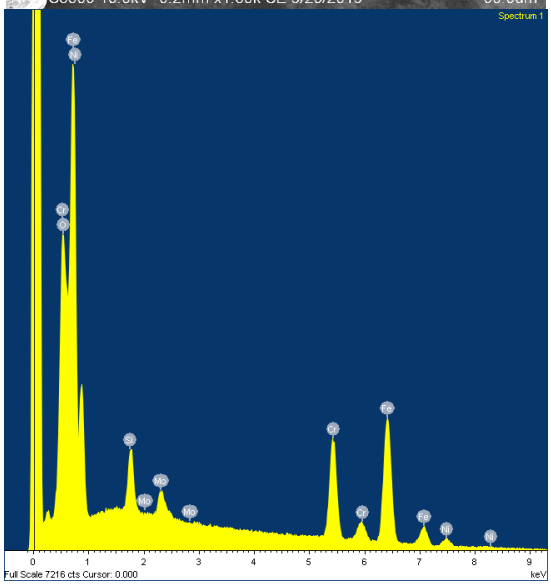

Element	Atomic%
Fe	52.30
Ni	13.82
Cr	16.27
O	14.17
Si	2.48
Mo	0.96

Figure 6 EDX comparison between the surface chemical composition of the virgin stainless steel powder (a) and spattered particles (b), the chemical information was extracted from a maximum x-ray penetration depth of approximately 100nm.

Figure 7 displays the XPS full survey spectra of the powders. High resolution spectra for Si, Cr, Fe and Ni are available in the supplementary document. Figure 7 indicates that the first few atomic layers of the surface of both powders are predominantly composed of oxygen and carbon. It was evident the presence of Si 2p and Si 2s peaks in both spatter and virgin powders. The analysis also indicated that the three main elements (Fe, Cr, and Ni) composing the powders are not present on their surfaces. This is common when performing XPS on stainless steel, both powders and solid layers, that the signal is dominated by signals from carbon and oxygen adsorbed on the surface. However, in this case it is not observed any other elemental

signals. This suggest that the surface contamination in the form of hydrocarbons and hydroxyls extends beyond the ca. 10 nm sampling depth of XPS. The golden colour effect was also achieved and reported by several studies which are focused on the surface melting of stainless steel in an open environment with the presence of oxygen for different applications like laser marking and engraving [43–47]. In order to be certain about this, further XPS investigation into the oxygen and silicon peaks is required and focus on any functional groups such as SiO_x and CO_x.

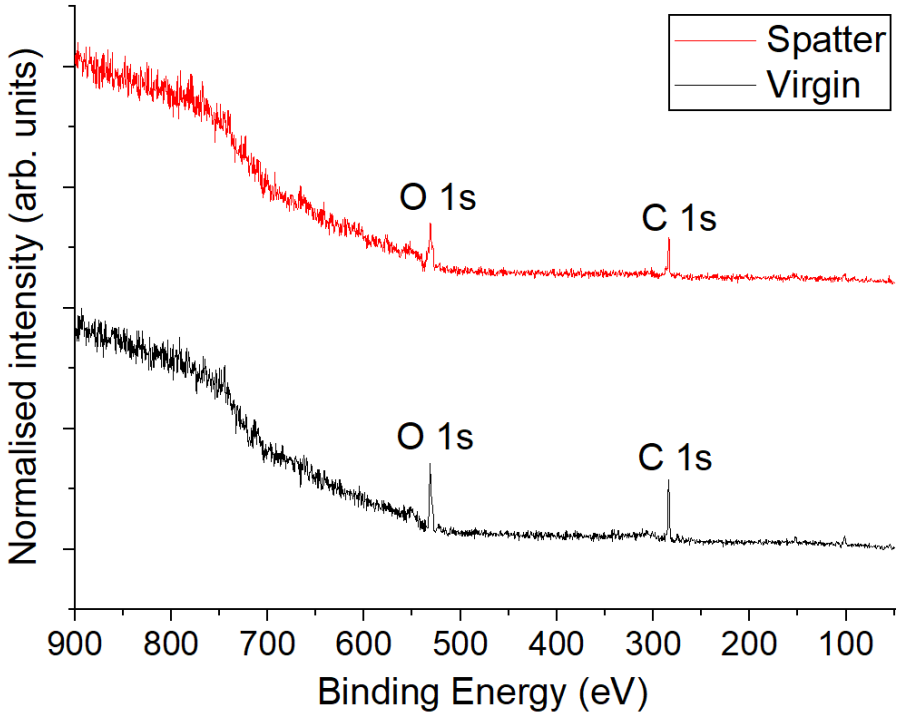

Figure 7 XPS full survey spectrum of the spatter and virgin 316L stainless steel powder.

3.3 Reflectance Spectroscopy

The virgin and the spattered powder were tested for their white light reflection properties. Figure 8 compares the spectra obtained from these powders. The spattered particles exhibit a clear reduction in the reflectivity between 500 and 900nm wavelength. It was also seen in Figure 2 (a) that the spattered powder presented a golden colouration and this could be the reason for improved light absorption. However, the reflection of the laser from a given powder depends on a series of factors such as particle morphology, chemical composition, oxidation condition and temperature, laser type and wavelength, and irradiation atmosphere. Therefore, in powder bed fusion, the absorption/reflection of light by metallic powders is a much more complex phenomenon.

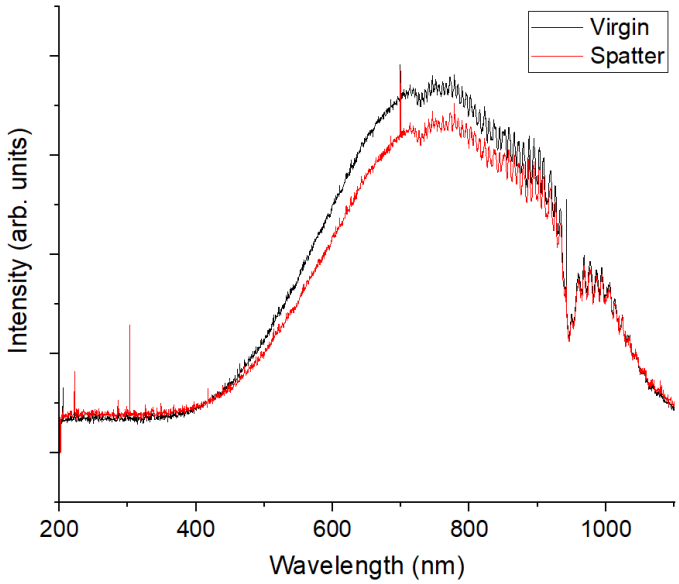

Figure 8 Reflectance spectra of the virgin and spattered powders particles.

3.4 Crystallographic Studies of Powders

Figure 9 shows the XRD patterns of virgin and spattered powder. The results indicate that all powder samples consist of face centered cubic systems with major peaks along the (111) and (200) orientations. There are no noticeable variations in the crystal structure between the powder indicating the fact that spatter formation did not introduce any crystal structure/phase variations in the bulk of the powder particle, although they went through a fast melting and solidification process. However, the presence of ultrathin amorphous layers or phase formation on the surface of the powder particles cannot be ruled out using XRD alone as it is a bulk analysis technique and will not be powerful enough to detect small surface variations.

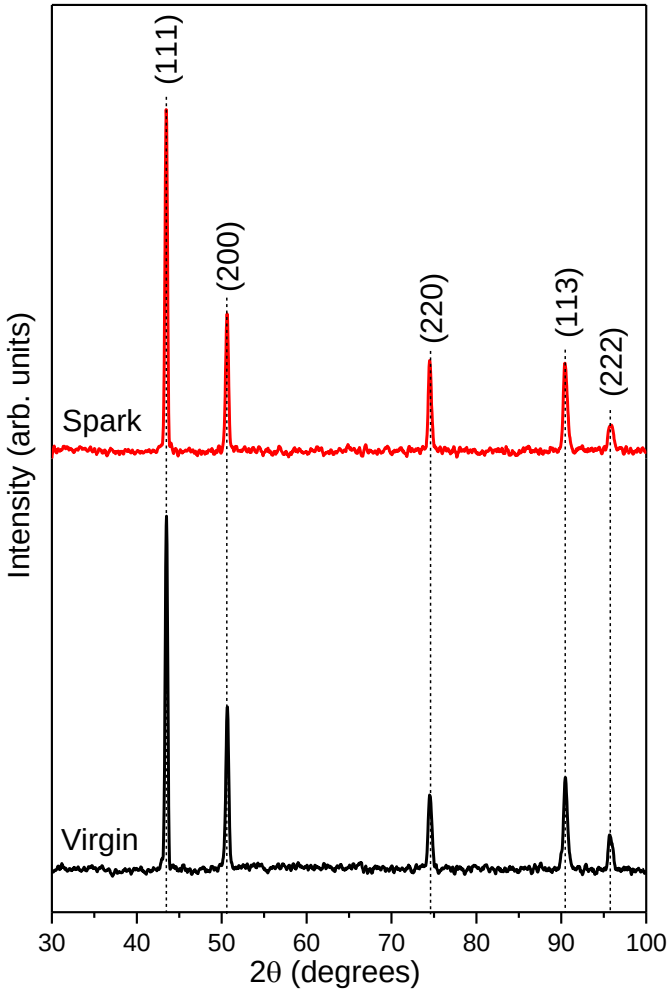

Figure 9 Normalised XRD patterns for virgin and spatter powders.

4. Conclusions

In this study, spatter generated during selective laser melting of 316L stainless steel was successfully characterised and benchmarked against the virgin powder. Spattered powder presented a very unique golden colouration due to reactions with the atmosphere and other contaminants during the virgin powder melting and solidification process. The morphology of laser spattered powder was found to be comprised of large irregularly shaped aggregates. Spattered powder residing on the printing area can prevent the next layer of powder from being deposited uniformly and may also cause internal defects in printing parts due to other factors. It was show that spattered powder is less dense which is due to closed internal porosities containing entrapped gasses or other contaminants. An increased specific surface area in the spatter is a result of numerous small satellites, roughness and distorted shape of this powder. Recyclability of virgin powder containing spatter is possible via sieving. Nevertheless, smaller spattered particles will pass through the sieve mesh, and even though this powder can now be mixed with virgin powder, printing a defect free-part is most likely to be achieved by using a feedstock composed of 100 % pure virgin powder.

The chemical composition extracted from the maximum depth of 100nm from the surface of the powders revealed that the atomic percentage of Fe, Ni and Cr, the main elements in the 316L stainless steel, changed substantially in the spattered powder. The EDX analysis also showed an increase of oxygen content on the spattered powder. The first few atomic layers of the surface of both powders were predominantly composed of oxygen and carbon. Si 2p and Si 2s peaks were also identified. However, the XPS high resolution spectra showed that the main elements composing the powders were not present on their surfaces. The high concentrations of oxygen found in both powders suggests the presence of a thin moisture film bonded on the surface of the powders. In order to identify the causes of golden coloration of the spattered powder, further investigation into the oxygen and silicon peaks is required and look for any structure within these peaks such as SiOx and COx. Large number of small satellite structures, roughness and the golden coloration chemistry of the spattered powder contributed to improving this powder light absorptivity for wavelengths between 500 and 900nm. The XRD results showed that spatter formation did not introduce any crystal structure/phase variations in the bulk of the powder particle.

Spatter is detrimental to building parts and also to powder recyclability. Spatter formation is unavoidable, but minimising its effect is possible through optimisation of parameters such as inert gas flow velocity and laser energy. However, an optimum condition that minimises spatter formations may not be suitable for printing a part with a specific metallographic structure for example. Further attention needs to be paid to this in order to understand how an optimum printing condition for spattering control influences part quality and properties.

The results presented in this study are of significant contribution to the powder bed fusion additive manufacturing field as they provide a unique insight to the characteristics of spatter matter generated from the processing of 316L stainless steel powder.

Acknowledgments

This publication has emanated from research supported by a research grant from Science Foundation Ireland (SFI) under grant number 16/RC/3872 and is co-funded under the European Regional Development Fund. Parts and samples for this project were manufactured using facilities in the Additive Research Laboratory at the AMBER centre, CRANN Institute, Trinity College Dublin, Ireland. The AR-Lab is an SFI supported research centre.

References

[1] Kruth, J. P., 1991, “Material Incress Manufacturing by Rapid Prototyping Techniques,” CIRP Annals, 40(2), pp. 603–614.
[2] Kruth, J.-P., Levy, G., Klocke, F., and Childs, T. H. C., 2007, “Consolidation Phenomena in Laser and Powder-Bed Based Layered Manufacturing,” CIRP Annals, 56(2), pp. 730–759.
[3] Guo, N., and Leu, M. C., 2013, “Additive Manufacturing: Technology, Applications and Research Needs,” Front. Mech. Eng., 8(3), pp. 215–243.
[4] van Noort, R., 2012, “The Future of Dental Devices Is Digital,” Dent Mater, 28(1), pp. 3–12.

[5] Scipioni Bertoli, U., Wolfer, A. J., Matthews, M. J., Delplanque, J.-P. R., and Schoenung, J. M., 2017, "On the Limitations of Volumetric Energy Density as a Design Parameter for Selective Laser Melting," Materials & Design, 113, pp. 331–340.
[6] Frazier, W. E., 2014, "Metal Additive Manufacturing: A Review," J. of Materi Eng and Perform, 23(6), pp. 1917–1928.
[7] Hull, C. W., 1986, "Apparatus for Production of Three-Dimensional Objects by Stereolithography."
[8] Wohlers, T., and Gornet, 2014, History of Additive Manufacturing: Introduction of Non-SL Systems Introduction of Low-Cost 3D Printers.
[9] Vayre, B., Vignat, F., and Villeneuve, F., 2012, "Metallic Additive Manufacturing: State-of-the-Art Review and Prospects," Mechanics & Industry, 13(2), pp. 89–96.
[10] Gokuldoss, P. K., Kolla, S., and Eckert, J., 2017, "Additive Manufacturing Processes: Selective Laser Melting, Electron Beam Melting and Binder Jetting-Selection Guidelines," Materials (Basel), 10(6).
[11] Hoeges, S., Lindner, M., Meiners, W., and Smeets, R., 2010, "Bioresorbable Implants Using Selective Laser Melting," pp. 908–920.
[12] Lykov, P. A., Baitimerov, R. M., Panfilov, A. V., and Guz, A. O., 2017, "The Manufacturing of TiAl6V4 Implants Using Selective Laser Melting Technology," IOP Conference Series: Materials Science and Engineering, Seoul, South Korea.
[13] Wang, H., Zhao, B., Liu, C., Wang, C., Tan, X., and Hu, M., 2016, "A Comparison of Biocompatibility of a Titanium Alloy Fabricated by Electron Beam Melting and Selective Laser Melting," PLOS ONE, 11(7).
[14] Wauthle, R., van der Stok, J., Amin Yavari, S., Van Humbeeck, J., Kruth, J.-P., Zadpoor, A. A., Weinans, H., Mulier, M., and Schrooten, J., 2015, "Additively Manufactured Porous Tantalum Implants," Acta Biomater, 14, pp. 217–225.
[15] Wagner, S. M., and Walton, R. O., 2016, "Additive Manufacturing's Impact and Future in the Aviation Industry," Production Planning & Control, 27(13), pp. 1124–1130.
[16] Uhlmann, E., Kersting, R., Klein, T. B., Cruz, M. F., and Borille, A. V., 2015, "Additive Manufacturing of Titanium Alloy for Aircraft Components," Procedia CIRP, 35, pp. 55–60.
[17] F42 Committee, 2015, Terminology for Additive Manufacturing Technologies, ASTM International.
[18] Lykov, P., Baytimerov, R., Vaulin, S., Safonov, E., and Zherebtsov, D., 2016, Selective Laser Melting of Copper by 200 W CO2 Laser, 2016, SAE International, Warrendale, PA.
[19] Popovich, A., Sufiiarov, V., Polozov, I., Borisov, E., Masaylo, D., and Orlov, A., 2016, "Microstructure and Mechanical Properties of Additive Manufactured Copper Alloy," Materials Letters, 179, pp. 38–41.
[20] Rong, T., and Gu, D., 2016, "Formation of Novel Graded Interface and Its Function on Mechanical Properties of WC1−x Reinforced Inconel 718 Composites Processed by Selective Laser Melting," Journal of Alloys and Compounds, 680, pp. 333–342.
[21] Liu, H., Su, H., Shen, Z., Wang, E., Zhao, D., Guo, M., Zhang, J., Liu, L., and Fu, H., 2018, "Direct Formation of Al2O3/GdAlO3/ZrO2 Ternary Eutectic Ceramics by Selective Laser Melting: Microstructure Evolutions," Journal of the European Ceramic Society, 38(15), pp. 5144–5152.
[22] Gibson, I., David W., R., and Stucker, B., 2010, Additive Manufacturing Technologies: Rapid Prototyping to Direct Digital Manufacturing, Springer.
[23] Thijs, L., Verhaeghe, F., Craeghs, T., Humbeeck, J. V., and Kruth, J.-P., 2010, "A Study of the Microstructural Evolution during Selective Laser Melting of Ti–6Al–4V," Acta Materialia, 58(9), pp. 3303–3312.

[24] Amato, K. N., Gaytan, S. M., Murr, L. E., Martinez, E., Shindo, P. W., Hernandez, J., Collins, S., and Medina, F., 2012, "Microstructures and Mechanical Behavior of Inconel 718 Fabricated by Selective Laser Melting," Acta Materialia, 60(5), pp. 2229–2239.
[25] Tolosa, I., Garciandía, F., Zubiri, F., Zapirain, F., and Esnaola, A., 2010, "Study of Mechanical Properties of AISI 316 Stainless Steel Processed by 'Selective Laser Melting', Following Different Manufacturing Strategies," Int J Adv Manuf Technol, 51(5), pp. 639–647.
[26] Brandl, E., Heckenberger, U., Holzinger, V., and Buchbinder, D., 2012, "Additive Manufactured AlSi10Mg Samples Using Selective Laser Melting (SLM): Microstructure, High Cycle Fatigue, and Fracture Behavior," Materials & Design, 34, pp. 159–169.
[27] Anwar, A. B., Ibrahim, I. H., and Pham, Q.-C., 2019, "Spatter Transport by Inert Gas Flow in Selective Laser Melting: A Simulation Study," Powder Technology, 352, pp. 103–116.
[28] Read, N., Wang, W., Essa, K., and Attallah, M. M., 2015, "Selective Laser Melting of AlSi10Mg Alloy: Process Optimisation and Mechanical Properties Development," Materials & Design (1980-2015), 65, pp. 417–424.
[29] Wang, D., Wu, S., Fu, F., Mai, S., Yang, Y., Liu, Y., and Song, C., 2017, "Mechanisms and Characteristics of Spatter Generation in SLM Processing and Its Effect on the Properties," Materials & Design, 117, pp. 121–130.
[30] Qiu, C., Panwisawas, C., Ward, M., Basoalto, H. C., Brooks, J. W., and Attallah, M. M., 2015, "On the Role of Melt Flow into the Surface Structure and Porosity Development during Selective Laser Melting," Acta Materialia, 96, pp. 72–79.
[31] Taheri Andani, M., Dehghani, R., Karamooz-Ravari, M. R., Mirzaeifar, R., and Ni, J., 2018, "A Study on the Effect of Energy Input on Spatter Particles Creation during Selective Laser Melting Process," Additive Manufacturing, 20, pp. 33–43.
[32] Gasper, A. N. D., Szost, B., Wang, X., Johns, D., Sharma, S., Clare, A. T., and Ashcroft, I. A., 2018, "Spatter and Oxide Formation in Laser Powder Bed Fusion of Inconel 718," Additive Manufacturing, 24, pp. 446–456.
[33] Khairallah, S. A., Anderson, A. T., Rubenchik, A., and King, W. E., 2016, "Laser Powder-Bed Fusion Additive Manufacturing: Physics of Complex Melt Flow and Formation Mechanisms of Pores, Spatter, and Denudation Zones," Acta Materialia, 108, pp. 36–45.
[34] Bidare, P., Bitharas, I., Ward, R. M., Attallah, M. M., and Moore, A. J., 2018, "Fluid and Particle Dynamics in Laser Powder Bed Fusion," Acta Materialia, 142, pp. 107–120.
[35] Ly, S., Rubenchik, A. M., Khairallah, S. A., Guss, G., and Matthews, M. J., 2017, "Metal Vapor Micro-Jet Controls Material Redistribution in Laser Powder Bed Fusion Additive Manufacturing," Scientific Reports, 7(1), pp. 1–12.
[36] Gunenthiram, V., Peyre, P., Schneider, M., Dal, M., Coste, F., Koutiri, I., and Fabbro, R., 2018, "Experimental Analysis of Spatter Generation and Melt-Pool Behavior during the Powder Bed Laser Beam Melting Process," Journal of Materials Processing Technology, 251, pp. 376–386.
[37] Sutton, A. T., Kriewall, C. S., Leu, M. C., Newkirk, J. W., and Brown, B., 2020, "Characterization of Laser Spatter and Condensate Generated during the Selective Laser Melting of 304L Stainless Steel Powder," Additive Manufacturing, 31.
[38] Anwar, A. B., and Pham, Q.-C., 2018, "Study of the Spatter Distribution on the Powder Bed during Selective Laser Melting," Additive Manufacturing, 22, pp. 86–97.
[39] Liu, Y., Yang, Y., Mai, S., Wang, D., and Song, C., 2015, "Investigation into Spatter Behavior during Selective Laser Melting of AISI 316L Stainless Steel Powder," Materials & Design, 87, pp. 797–806.

[40] Esmaeilizadeh, R., Ali, U., Keshavarzkermani, A., Mahmoodkhani, Y., Marzbanrad, E., and Toyserkani, E., 2019, "On the Effect of Spatter Particles Distribution on the Quality of Hastelloy X Parts Made by Laser Powder-Bed Fusion Additive Manufacturing," Journal of Manufacturing Processes, 37, pp. 11–20.
[41] Low, D. K. Y., Li, L., and Corfe, A. G., 2000, "Effects of Assist Gas on the Physical Characteristics of Spatter during Laser Percussion Drilling of NIMONIC 263 Alloy," Applied Surface Science, 154–155, pp. 689–695.
[42] Sola, A., and Nouri, A., 2019, "Microstructural Porosity in Additive Manufacturing: The Formation and Detection of Pores in Metal Parts Fabricated by Powder Bed Fusion," Journal of Advanced Manufacturing and Processing, 1(3).
[43] Kučera, M., Švantner, M., and Smazalová, E., 2014, "Influence of Laser Marking on Stainless Steel Surface and Corrosion Resistance," Lasers in Manufacturing Conference.
[44] Lu, Y., Shi, X., Huang, Z., Li, T., Zhang, M., Czajkowski, J., Fabritius, T., Huttula, M., and Cao, W., 2017, "Nanosecond Laser Coloration on Stainless Steel Surface," Scientific Reports, 7(1), pp. 1–8.
[45] Laakso, P., Pantsar, H., and Mehtälä, V., 2008, Marking Decorative Features to Stainless Steel with Fiber Laser, 1VTT Technical Research Centre, Finland, Fraunhofer USA Inc. Center for Laser Technology.
[46] Ming, L., Hoult, A., and Tse, A., 2008, "Colour Marking of Metals with Fiber Lasers," PICALO, 2008(1), pp. 67–70.
[47] Zheng, H. Y., Lim, G. C., Wang, X. C., Tan, J. L., and Hilfiker, J., 2002, "Process Study for Laser-Induced Surface Coloration," Journal of Laser Applications, 14(4), pp. 215–220.